Received 8 June 2023, accepted 16 July 2023, date of publication 26 July 2023, date of current version 3 August 2023.
Digital Object Identifier 10.1109/ACCESS.2023.3299226

APPLIED RESEARCH

Scaling Switching-Sequence-Based Control for Networked Power Converters

MATEO D. ROIG GREIDANUS[1], (Graduate Student Member, IEEE), SUDIP K. MAZUMDER[1], (Fellow, IEEE), DEBANJAN CHATTERJEE[2], (Member, IEEE), MUHAMMAD TAHIR[3], (Member, IEEE), AND NANDITHA GAJANUR[1], (Graduate Student Member, IEEE)
[1]Department of Electrical and Computer Engineering, University of Illinois Chicago (UIC), Chicago, IL 60607, USA
[2]ABB Corporate Research Center, Raleigh, NC 27606, USA
[3]Department of Electrical Engineering, Al-Khwarizmi Institute of Computer Science, University of Engineering and Technology at Lahore, Lahore 54890, Pakistan

Corresponding author: Sudip K. Mazumder (mazumder@uic.edu)

This work was supported in part by the U.S. Department of Energy's Office of Energy Efficiency and Renewable Energy under Solar Energy Technology Office under Award DE-EE0009026 and Award DE-CR0000019, and in part by the U.S. National Science Foundation under the Division Of Computer and Network Systems under Award 2219734.

ABSTRACT The control of networked power-electronics systems (PESs) using predictive switching sequences has been described in this paper. The switching-sequence-based control (SBC), first introduced in Mazumder and Acharya (2008), applies converter switching sequences to an optimization cost function to be satisfied under stability bounds. To evaluate the SBC control scalability and efficacy, the control strategy is implemented for centralized and distributed network architectures for different PES topologies. Given the two network architectures, dynamic and steady-state performances obtained using SBC are discussed using two different case illustrations: for a standalone and network of parallel hybrid active neutral-point-clamped (H-ANPC) inverters; and for a standalone and network of parallel differential-mode Ćuk rectifiers (DMCRs). Hence, the work highlights the feasibility of extending the SBC control application to PESs networks subject to communication constraints and latency dependencies.

INDEX TERMS Switching-sequence-based control (SBC), converter, power electronics, network.

I. INTRODUCTION

Networked power electronics systems (PES) are the foundation of today's power system applications. They provide flexibility in integrating distributed energy resources while easing voltage and current scaling [2]. Networked-connected PES also offers reliable, low-cost, and efficient power distribution solutions for load-sharing in an electrical grid [3]. For instance, some work in uninterrupted power supplies (UPS) [4] emphasizes the need for a network multi-inverter system to ensure steady operation while meeting the increasing power demand. Regarding control techniques, centralized control [5], master-follower control [6], current distribution control [7], and voltage droop controllers [8] and commonly employed for achieving regulated voltage and load sharing in networked PES systems. Nevertheless, ensuring these systems' overall stability and robustness can be challenging [9]. The challenges mainly stem from delays introduced by the communication between the networked PESs [10]. This latency makes them operate differently from the standalone time-invariant condition. As a problem-amplifying factor, the commonly applied multiple-timescale control strategies generally do not comprise the overall dynamic network model of the system. On account of that, [11] presents the urgent demand for novel control-oriented dynamic model aggregation techniques to ensure the stability of PES networks.

A PES is typically modeled using an averaged model to simplify dealing with dynamics, stability, and control design [12], [13], [14]. This leads to the conventional approach of treating control and modulation (which translates the smooth control output to a predefined switching sequence) separately [13], [14]. In SBC, this limitation is

The associate editor coordinating the review of this manuscript and approving it for publication was Zhilei Yao.

addressed by treating a PES as a hybrid dynamical system that facilitates the unification of control and modulation, thereby directly evolving the PES switching sequence based on a defined closed-loop control goal. Initially, using a recently defined work of the authors, the total number of feasible switching sequences of a PES is determined. Subsequently, a subset of these feasible switching sequences, referred to as the reachable switching sequences, is determined using a multiple- Lyapunov-function methodology [1]. Finally, an evolving optimal switching sequence is selected (out of these reachable switching sequences) to attain the desired control objective for the PES while ensuring robust stability. Even though sliding-mode and model-predictive controls [15], [16], [17], [18] also unify control and modulation, unlike the SBC, they primarily control the PES switching states while the switching sequence evolves with time. Besides, unlike the aforementioned control strategies, the SBC control provides the advantage of offline predetermination on the set of feasible switching sequences that can easily be extended to more sophisticated systems.

Extension of the SBC from standalone to networked PESs brings control distribution issues. SBC relies on a communication network for the exchange of control information. Important design issues include the choice of the implemented architectures based on computational and communication requirements [19], [20], [21], [22], [23]. One of them, the centralized control, is similar to the standalone control except that control feedback and actuation signals must be exchanged between the central controller and the various PES modules [20]. On the other hand, distributed control relies on coordination among the local controllers [20], [24], [25]. This introduces delays that need to be compensated so as to avoid degradation in the stability and performance of the PES network [26], [27], [28].

Given the advantages of SBC control over other linear [12] and model-predictive control strategies, this work contributes to the existing literature outlining the scalability of SBC control for PES network architectures. Analytical decomposition of the networked model and results in two different topologies support the SBC use for comprehensive PES network applications. This paper is outlined as follows. Section II outlines the mechanism of the SBC for the PES network, where the scalability of the control architectures and mechanisms for decomposing the system models for distributed implementations are investigated. Afterward, Section III briefly discussed the synthesis of the SBC control algorithm scheme for the PES network. Finally, in Section IV, the efficacy of SBC has been validated using the following two case illustrations: a) for standalone and parallel-connected H-ANPC inverters; and b) for standalone and parallel-connected DMCRs.

II. SBC FOR NETWORKED PES

Herein is a brief outline of the network for power electronics systems (PES) implementation is provided. Subsequently, mechanisms for the network model decomposition are outlined.

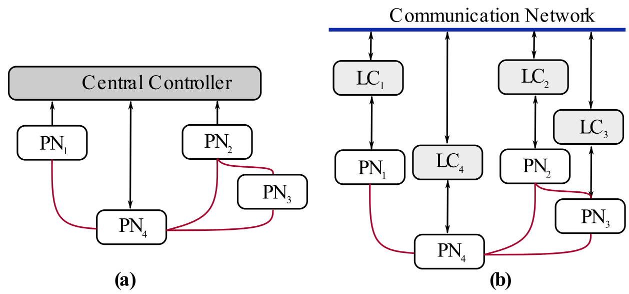

FIGURE 1. Illustrations of the architectures for implementation of the SBC for networked PESs: (a) centralized, (b) distributed control architectures. Symbol definitions: PN: power network and L.C.: local controller.

A. PES NETWORK ARCHITECTURES

Two different existing desynchronized network control strategies for load-sharing inverters are shown in Figure 1. In the centralized architecture for SBC [29], [30], as illustrated in Figure 1.(a), the entire PES network is treated as a single entity. State variables of all the modules are transmitted to a central controller. Using this information and knowledge of the overall network model, the central controller computes the optimal switching sequence and the time spent in each switching state of the sequence. This information is transmitted to all modules via a common broadcast through the communication network.

As illustrated in Figure 1.(b), for the distributed implementation architecture, the overall control problem for the PES network is decomposed into multiple local control problems [20], [22]. However, communication among the modules is needed to solve the local control problems. On that account, each module is affected by interactions with the remainder of the PES network. The local control scheme for each PES module is divided into the following steps: a) obtain current-sharing information from other modules; b) solve the optimization problem using local measurements and information from other modules, and c) send updated state information to the other modules.

Next, the scalability of the approaches is discussed. The total number of converter states (X), switching states (M), and switching sequences (L) of a PES network with N modules for centralized and distributed SBC implementations are provided. For the centralized control scheme, X, M, and L are, respectively, found to be $X = \sum_{j=1}^{N} \text{size}\left(x_j\right)$, $M = 2^{\sum_{j=1}^{N} S_j} - \sum_{j=1}^{N} W_j$, and $L = \sum_{l=1}^{M} M_{C_l}$ while for the distributed control the same parameters are, respectively, found to be $X = \text{size}\left(x_j\right)$, $M = 2^{S_j} - W_j$, and $L = M_{C_l}$. Here, x_j, S_j, and W_j represent the states, number of non-complementary switching functions, and the number of redundant switching states of the j^{th} module of the network, respectively, and size $\left(x_j\right)$ represents the size of the vector x_j. C_l regards to the combination of l sequences given M such that $M_{C_l} = (M!)\big/\left(l!\left((M-l)!\right)\right)$, as discussed in [1].

The variations of the communication and computational requirements for the architectures are based on the following assumptions:

- the number of switching sequences proportionally impacts the computational requirement;
- the overall communication requirement is directly proportional to the number of variables that must be exchanged;
- all the modules are in proximity, that can yield channel interference in the presence of simultaneous communication; as such, a time-division multiple access protocol [31] is selected for inter-module communication.

Further, the additional computational overhead required for synchronization among the PES modules and the central controller [32] is ignored. It is noted that, despite the assumptions made in the analysis presented in this section, the general conclusions drawn from the outlined results apply to other large-scale networks [33], [34] with different time constants and different power ratings, provided that the controller has information on the overall system model.

B. PES MODEL DECOMPOSITION FOR CENTRALIZED AND DISTRIBUTED ARCHITECTURES

For centralized SBC implementation, the overall PES-network model is described first. The decomposition of this model for distributed implementation is outlined next. Reference [27] provides the parametric and matrix details for the models.

The piecewise-linear (PWL) hybrid dynamical model of the PES network, which is used for the centralized SBC is described by the following vector differential equation:

$$\dot{x}(t) = A_i x(t) + B_i. \tag{1}$$

where $x(t) = (x_1(t)\, x_2(t) \cdots x_N(t))^T$ represents the states of the N-module PES network. In (1), $x_1(t)$, $x_2(t)$, $\cdots$, $x_N(t)$ represent the states of each module, i represents the cumulative switching states of the PES network, and the matrix A_i and vector B_i are expressed as follows:

$$A_i = \begin{bmatrix} A_{11_i} & A_{12_i} & \cdots & A_{1N_i} \\ \vdots & & \ddots & \vdots \\ A_{N1_i} & A_{N2_i} & \cdots & A_{NN_i} \end{bmatrix} \text{ and } B_i = \begin{bmatrix} B_{1_i} \\ \vdots \\ B_{N_i} \end{bmatrix}.$$

The off-diagonal elements of the A_i matrix represents the coupling between the various PES modules of the network, while the diagonal elements of A_i represent the decoupled system. In the absence of the off-diagonal elements, a wholly decoupled model of the network is realized, and a decentralized control scheme, devoid of intra-network communication, suffices. The independent B_i matrix represents the feedthrough elements of the PES network dynamical model.

From (1), the local PWL model of the j^{th} PES module is expressed as follows:

$$x_j(t) = A_{j1_{i'}} x_j(t) + B_{j_{i'}} + \sum\nolimits_{k=1,k\neq j}^{N} A_{jk_{i'}} x_k(t) \tag{2a}$$

where $x_j(t)$ represents the states of the module, $A_{j1_{i'}}$ and $B_{j_{i'}}$ are matrices and vectors of appropriate dimensions, and i' represents the switching states of the j^{th} module. The term $\sum_{k=1,k\neq j}^{N} A_{jk_{i'}} x_k(t)$ represents the coupling of the j^{th} PES module with the remainder of the PES network. For the distributed control implementation, information regarding the states of the other PES modules ($x_k(t)$) is obtained via the communication network. Owing to the inherent communication-network time delays, the local (2a) has to be modified and is expressed as follows:

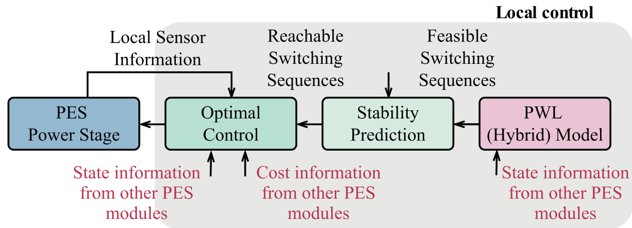

FIGURE 2. SBC control flow for a distributed architecture. The local controller receives information from other modules aside from sending information to other modules (which is not shown).

$$\dot{x}_j(t) = A_{j1_{i'}} x_j(t) + B_{j_{i'}} + \sum\nolimits_{k=1,k\neq j}^{N} A_{jk_{i'}} x_k\left(t - \tau_{jk}\right). \tag{2b}$$

In (2b), τ_{jk} is the time delay experienced in transmitting the information of the state(s) of the k^{th} PES module to the j^{th} PES module over the communication network. The stability techniques described in [1] can be applied to determine the stability bounds of (2b).

III. SYNTHESIS OF SBC SCHEME FOR THE PES NETWORK

The general SBC control strategy, introduced in [1], comprises three key elements: a hybrid model representation of a PES, a set of switching sequences of the PES, and a composite Lyapunov function-based stability criterion. The basic methodology initiates with using the switching sequences and the hybrid model to ascertain a subset of feasible switching sequences that ensure convergence (reachability) of state trajectories for orbital motion. Subsequently, a union of feasible switching sequence(s) is so selected that an optimization cost function is satisfied under stability bound. The optimization process also yields the time duration of the applied feasible sequences and the allocation of this time among the switching states. The mechanism for centralized SBC implementation for the PES network, modeled by (1), is obtained by solving the optimal control problem that feeds switching sequences for the PES network. The sets of feasible switching sequences for the centralized or distributed implementation are obtained, respectively, using the models (1), (2a), and a combination of (1) and (2b) and using the multiple-Lyapunov-function-based methodology, described in [1]. The methodology described in the aforementioned paper describes in detail the stability analyses technique to determine the reachability bounds with variations of the number of modules and time delays, which can be straightforwardly applied here to determine the sets of feasible switching sequences from (2a) and (2b).

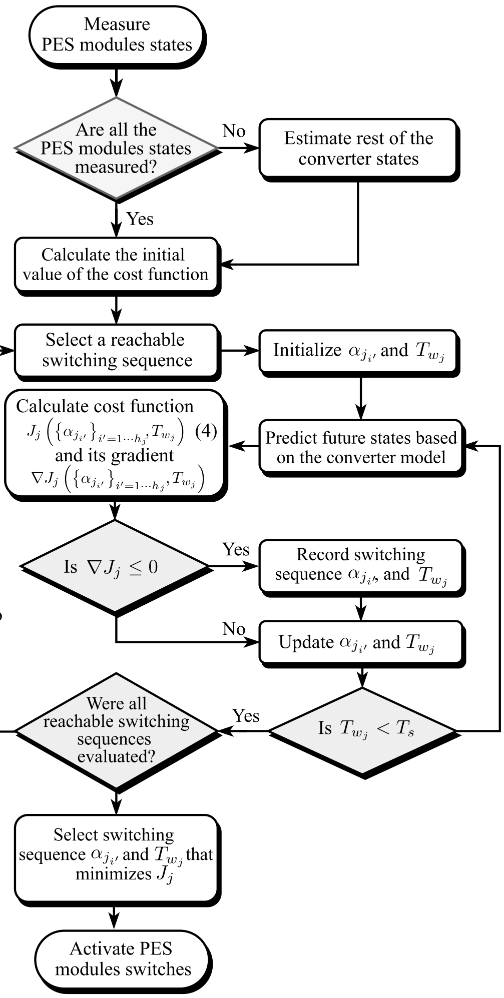

FIGURE 3. Outline of the control flow for the SBC of the distributed networked PES module.

The control problem must be distributed among the various PES modules for the distributed implementation. As manifested in Figure 2, this requires the decomposition of the centralized SBC problem into N sub-problems that can be solved using a combination of information from other modules of the PES network and local state feedback. This methodology is captured in Figure 3.

The first step for the implementation of the SBC optimal control is to determine a map projecting the states of the network PES over a time horizon T_{w_j} (i.e.,$x_j\left(t_0+T_{w_j}\right)$) based on an initial measurement of the states ($x_j\left(t_0\right)$). Hence, the local j^{th} PES module, the local state feedback $x_j\left(t\right)$ and information from other PES modules $.\tau\left\{x_k\left(t - {}_{jk}\right)\right\}_{k\neq j}$ along with the knowledge of the local model (and models of the interconnection), are used to determine the discrete map of the local module:

$$x_j\left(t_0+T_{w_j}\right) = f_j\left(\begin{array}{l} x_j\left(t_0\right), \left\{\alpha_{j_{i'}}\right\}_{i'=1\cdots h_j}, T_{w_j}, \left\{A_{j1_{i'}}\right\}_{i'=1\cdots h_j}, \\ \left\{B_{j_{i'}}\right\}_{i'=1\cdots h_j}, \sum_{k=1,k\neq j}^{N} A_{jk_{i'}} x_k\left(t-\tau_{jk}\right) \end{array}\right). \qquad (3)$$

where T_{w_j} is the time horizon (i.e., time duration of the prediction horizon), and $\left\{\alpha_{j_{i'}}\right\}_{i'=1\cdots h_j}$ is the proportion of T_{w_j} spent in each i' switching states of a total number of h_j for the j^{th} module. $f_j\left(.\right)$ denotes a function of $\left(.\right)$ that composes the for the discrete map $x_j\left(t_0+T_{w_j}\right)$.

Subsequently, the distributed optimization problem is expressed by the objective that follows:

Determine $\left\{\alpha_{j_{i'}}\right\}_{i'=1\cdots h_j}$ and T_{w_j} that minimizes the cost function

$$J_j\left(\left\{\alpha_{j_{i'}}\right\}_{i'=1\cdots h_j}, T_{w_j}\right) = \left(x_j^* - x_j\left(t_0+T_{w_j}\right)\right)^T P_j\left(x_j^* - x_j\left(t_0+T_{w_j}\right)\right)$$

such that

$$\begin{aligned} &x_j\left(t_0+T_{w_j}\right) = f_j\left(.\right) \\ &x_j\left(t_0+T_{w_j}\right) \leq x_{j\max} \\ &\sum_{i'=1}^{h_j} \alpha_{j_{i'}} = 1, \quad 0 < \alpha_{j_{i'}} \leq 1,\ i' = 1\cdots h_j \end{aligned} \qquad (4)$$

where $x_{j\max}$ represents the maximum values that the network states can attain and P_j is a positive-definite diagonal matrix and x_j^* is the control reference of the objective function. The values of x_j^* can be fixed or a function of other PES-network states $\left(\text{i.e., } x_j^* = g_j\left(x_j\left(t_0\right), \left\{x_k\left(t-\tau_{jk}\right)\right\}_{k=1,k\neq j}^{k=N}\right)\right)$. For example, to achieve load sharing in parallel H-ANPC inverters, as shown in Figure 4, each module's current reference may be the average value of all the module currents. Finally, the optimization in (4) is solved using quadratic programming algorithms [35], [36].

IV. RESULTS

The effectiveness of the SBC is explored here for two different case illustrations. It is explored initially for a voltage source PES (VS-PES) single-phase H-ANPC inverter network and then for current sources PES (CS-PES) differential-mode Ćuk rectifiers. The two illustration cases presented below aim to support the previously presented control strategy's findings and verify the SBC strategy's scalability for centralized and distributed network strategies. The communication delays differentiate the centralized and distributed network schemes in terms of computational effort, communication bandwidth requirements, and dynamic convergence. In the end, results with the differential data transfer ensure better performance of the PES network utilizing SBC.

A. CASE ILLUSTRATION OF STANDALONE AND NETWORKED SBC FOR SINGLE-PHASE HYBRID SWITCHING ANPC INVERTERS

This case illustration evaluates the application of the SBC controller to a single-phase H-ANPC inverter network. This example is implemented using a TMS320F28335 microcontroller to compute the SBC control scheme. The OPAL-RT real-time simulation (RTS) platform is used to emulate the H-ANPC inverter network performing load sharing, as is

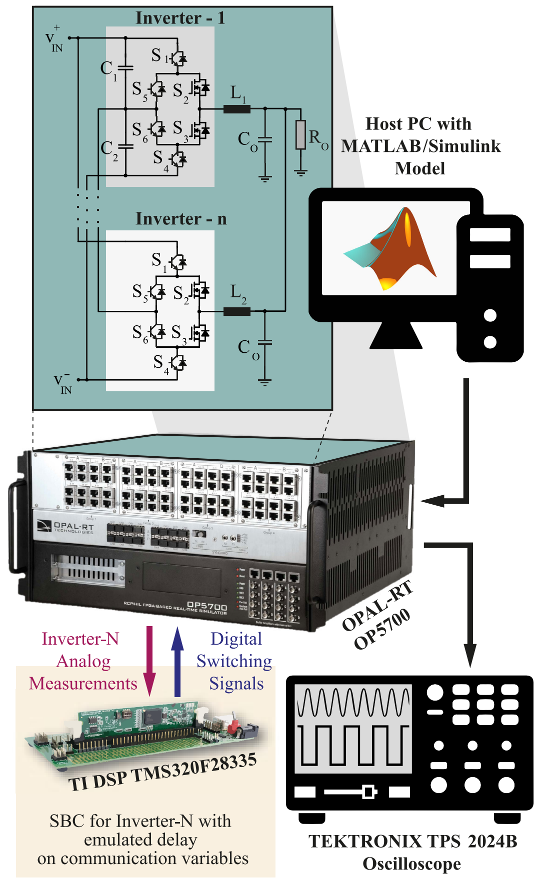

FIGURE 4. Real-time simulation schematic for case illustration of Standalone and Networked load-sharing SBC for single-phase H-ANPC.

TABLE 1. Single-phase H-ANPC parameters.

Input voltage (V_{DC})	Output voltage range (V_{out})	Input inductance (L_F)
800 V	600 Vpp	150 μH
Output capacitor (C_F)	Switching frequency (f_N/f_S)	Resistive Load (R_O)
10 μF	60 Hz / 42 kHz	20 Ω
Switches characteristics		Power rating
two FET (SiC) & four IGBT (Si) per module		1 kW per module

FET stands for field-effect transistor and IGBT regards insulated-gate bipolar transistor, using SiC (Silicon Carbide) and traditional Si (Silicon) semiconductor technologies, respectively.

shown in Figure. 4. The nominal values of the single-phase H-ANPC inverter are specified in Table 1.

FET stands for field-effect transistor and IGBT regards insulated-gate bipolar transistor, using SiC (Silicon Carbide) and traditional Si (Silicon) semiconductor technologies, respectively.

The SBC control strategy for the system acts on the current of each inverter that follows a load-sharing current reference.

The following cost function governs the dynamics of the system:

$$J_j=\sigma_1\left(\frac{1}{N}\left(\begin{array}{l} i_{o_j}\left(t_0+T_{w_j}\right) \\ +\sum_{k=1,k\neq j}^{N} i_{o_k}\left(t_0+T_{w_j}-\tau_{jk}\right)\end{array}\right)-i_{o_j}\left(t_0+T_{w_j}\right)\right)^2 +\sigma_2\left(v_{NP}\left(t_0+T_{w_j}\right)\right)^2 \quad (5)$$

where σ_1 and σ_2 are weighting factors, i_o refers to Inverter-N output current, and v_{NP} concerns to the neutral point voltage on the D.C. link of the parallel inverters.

The cost function in (5) is, herein, the performance measure that weighs the error between the expected reference. $\left(\text{i.e.,} i_{o_j}^* = g_j\left(i_{o_j}(t_0), \left\{i_{o_j}\left(t-\tau_{jk}\right)\right\}_{k=1,k\neq j}^{k=N}\right)\right)$ and the projected output current states of the H-ANPC inverter module $\left(\text{i.e.,} i_{o_j}\left(t_0+T_{w_j}\right)\right)$. Additionally, the split capacitor voltage neutral point predictions $\left(\text{i.e.,} v_{NP}\left(t_0+T_{w_j}\right)\right)$ are also considered to ensure equal voltage balance on them, thus avoiding common-mode current circulation on the neutral ground reference. Provided the above, the optimization routine minimizes the cost function to guarantee optimal tracking performance such that

$$\begin{aligned} &\min J_j\left(\left\{\alpha_{jn_{i'}}\right\}_{i=1\cdots h,n=1,2}, \left\{T_w\right\}_{w=\{N,S\}}, \sigma_{1,2}, i_{o_{k+1}}, v_{NP_{k+1}}\right) \\ &s.t. \\ &\qquad \hookrightarrow (t_1^{\alpha_{j1_{i'}}} + t_2^{1-\alpha_{j1_{i'}}}) = T_N; \\ &\qquad\quad (t_3^{\alpha_{j2_{i'}}} + t_4^{1-\alpha_{j2_{i'}}}) = T_S \\ &\text{with} \quad \alpha_{j1_{i'}}, \alpha_{j2_{i'}} \in \mathbb{R} : [0, 1] \end{aligned} \quad (6)$$

where T_N corresponds to a 60 Hz frequency period, that drives the switches $S_1 \cup S_6$ ($\alpha_{j1_{i'}}$), and switches $S_4 \cup S_5$ (1-$\alpha_{j1_{i'}}$), respectively. T_S corresponds to the high switching frequency period that drives the switches $S_2\left(\alpha_{j2_{i'}}\right)$ and $S_2\left(1-\alpha_{j2_{i'}}\right)$.

The switching constraints applied to the optimization routine presented above place the H-ANPC system in a peculiar condition for networked load-sharing schemes in terms of stability boundaries. This case example aims to show that the choice of communication architecture should consider the network's ability to exchange data and the computational effort.

In addition to these aspects, the impact of communication latency on the system's dynamic performance must also be considered. The dynamic impact of the control strategy largely stems from the hybrid nature of inverter switching in this illustration case. ANPC-type hybrid inverters have low-frequency switching dynamics aligned to the system's common voltage line frequency. A delay in the communication between inverter control agents will inevitably result in a time mismatch between load-sharing currents and line frequency.

The SBC control, being an optimal control strategy, outperforms other linear control strategies by presenting a rapid response to transients in the system. For illustration purposes, Figure 5 shows the steady-state and transient behavior of the voltage waveform of three H-ANPC s in a centralized control network after a step in the voltage reference. As can be seen, the transition is almost immediate, with an imperceptible overshoot and minimal settling time. In the centralized scheme, the rise time performance for a transient step is even more abrupt due to the independence of the reference synthesis layer.

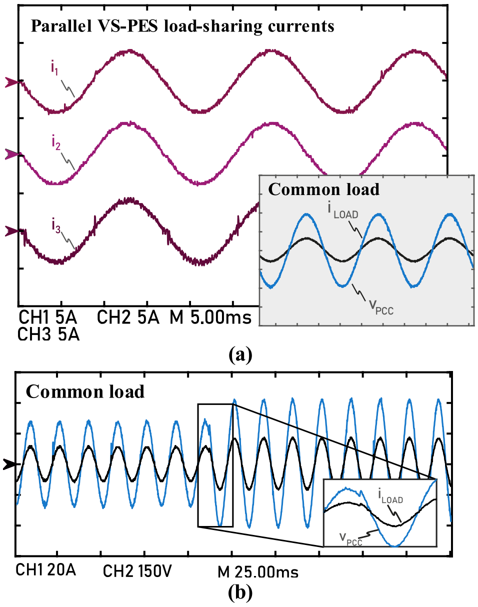

FIGURE 5. Load current and point of common coupling voltage waveforms to show a) the steady-state load-sharing currents of three parallel single-phase H-ANPC in centralized mode and b) the transient performance of the same load-sharing control strategies during a 50% voltage reference increase.

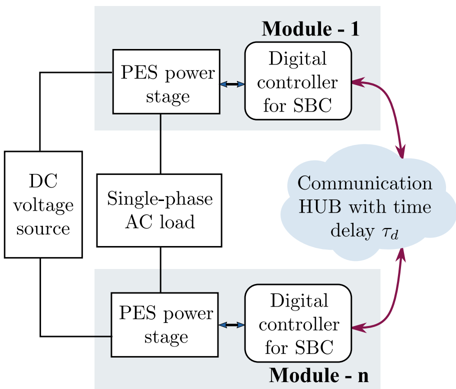

FIGURE 6. Schematic of a network comprising H-ANPC inverters connected in parallel. Here, only the distributed architecture for SBC implementation is illustrated.

Herein a network application involving multiple parallel-connected modules is outlined, as illustrated in Figure 6. For the distributed implementation, the H-ANPC inverters modules exchange their current information among themselves over a communication interface. The inherent time delays of such a network are considered while designing the parallel H-ANPC inverters network. Figure 7.(a)-(b) illustrates the centralized and distributed architectures for implementing the SBC for the parallel inverters ($N = 6$). A conventional broadcast-based time division multiplexing scheme is used. The transmission schedule is also illustrated for both cases. Here, ($k \rightarrow j$) represents a transmission from the kth module to the jth module.

Extending the analysis on the network architectures, Figure 8 shows that the total communication delay monotonically increases by the number of modules on the network. The figure also compares the delay-dependency behavior of the centralized and distributed network implementation for the H-ANPC inverters. With that, it illustrates that the communication requirements for the distributed implementation increase significantly with the number of modules, which may eventually violate the stability bounds of the system. The results also indicate that the stability threshold is higher in distributed network schemes, while the total network latency is superior to the centralized network architectures. The data exchanged by modules exponentially increases in distributed systems, unlike the linear growth perceived in centralized architectures, as shown in Figure 9. However, this discriminatory comparison must also consider the computational effort each methodology employs.

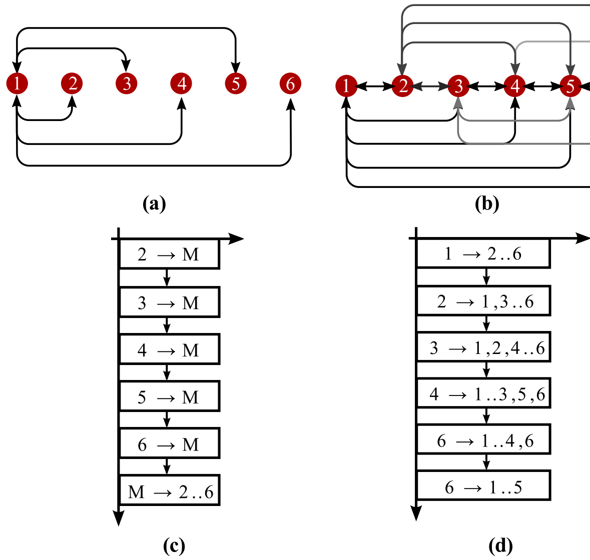

FIGURE 7. Schematics illustrating (a) a centralized and (b) a distributed architecture for the implementation of the SBC to a network consisting of six parallel VS-PESs. (c), (d) The respective transmission schedules for communication is also illustrated for both cases.

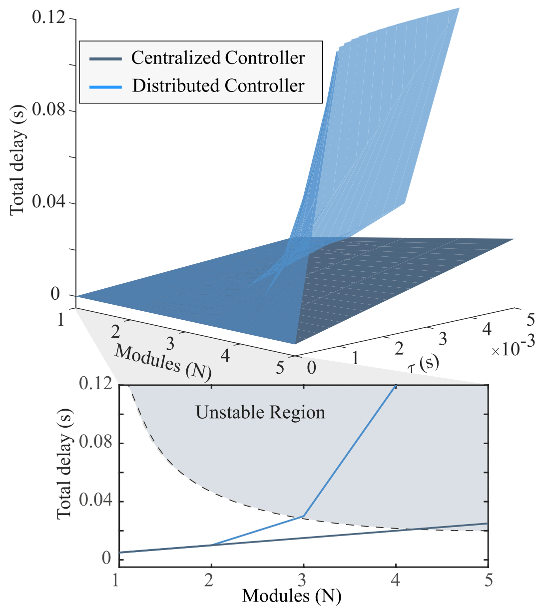

FIGURE 8. Total communication delay dependency by the number of modules in parallel and individual communication latency (τ).

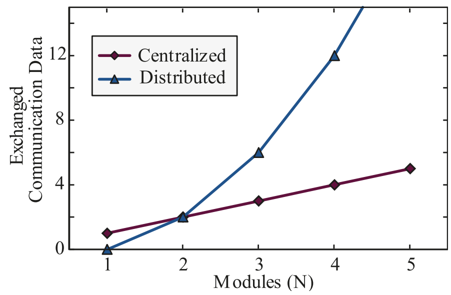

FIGURE 9. Comparison of the total exchanged communication data (in number of data packages) by transmission link per module with the centralized and distributed strategy for SBC.

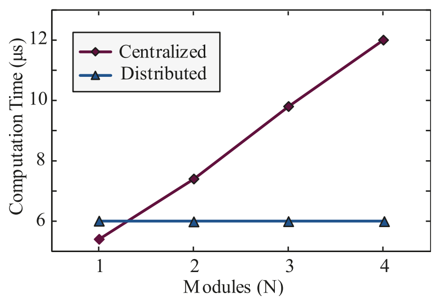

FIGURE 10. Comparison of the measured computation effort for each strategy.

TABLE 2. Single-phase DMCR parameters.

Input voltage (V_{in})	Output voltage range (V_{out})	Input inductance (L_1)	Output inductance (L_2)	Input capacitance (C_{in})
208 V RMS	400 V	50 μH	100 μH	10 μF
Output capacitance (C_{out})	Input blocking capacitance (C_1)	Output blocking capacitance (C_2)	Switching frequency ($1/T_s$)	Transformer turns ratio (N)
1 mF	6.8 μF	1.5 μF	20 kHz	2
Switches characteristics all FET (SiC) per module			Power rating 3.5 kW per module	

Distributed systems have a constant computational effort for solving the SBC problem, limited to the cascade control stages employed in the local controller as previously described in Figure 2. Conversely, centralized systems have a proportional relationship of the required computation effort to the number of modules employed in the scheme, as shown in Figure 10.

B. CASE ILLUSTRATION OF STANDALONE AND NETWORKED SBC FOR SINGLE-PHASE DMCR

The effectiveness of the SBC is explored now for a single-phase DMCR using the same procedure as with the H-ANPC. The nominal values of the DMCR have been specified in TABLE 2, and a network of n parallel DMCRs have been shown in Figure 11. The formulation of SBC for the standalone and paralleled DMCRs is similar to that of the single-phase H-ANPC inverters.

The efficacy of the SBC scheme to control a single module of the single-phase DMCR has been shown in Figure 12. Figure 12.(a) shows a comparative study of the convergence time of the input current of the DMCR for a traditional proportional-resonant (PR) compensator and SBC when a step change is given to the input current command. The PR compensator has been designed based on guidelines in [37].

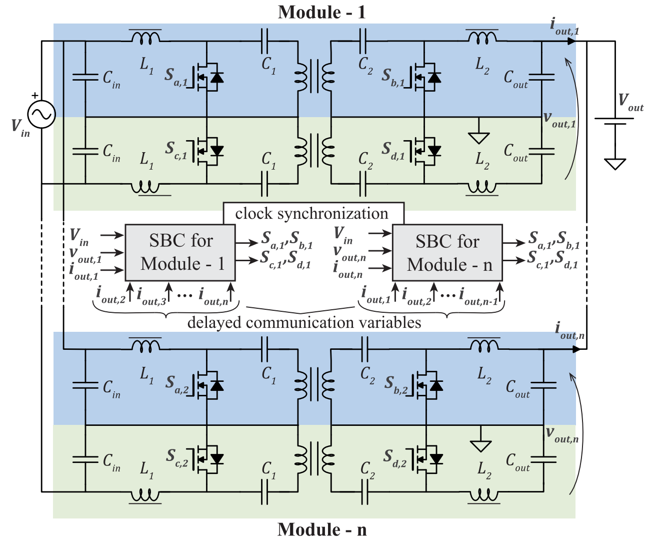

FIGURE 11. Network of n-parallel single-phase DMCRs.

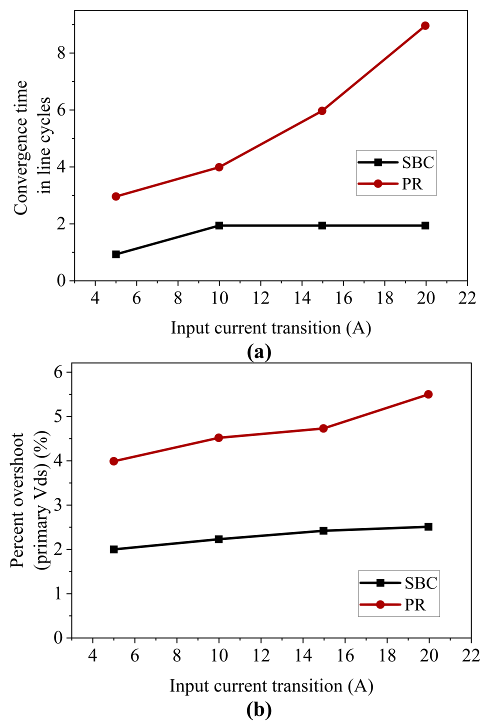

FIGURE 12. (a) Convergence time of the DMCR input current in terms of line cycles on a step change of the input current command with the same voltage overshoot of SBC as 2% nominal. (b) Figure showing that the increased gains of the linear controller to match the SBC response time leads to higher percent overshoot.

For both cases, the percent overshoot of the primary drain to source voltage for the step change has been kept at 2% of the nominal value. Since traditional controllers are based on reduced-order models of the actual system, they always give a trade-off between faster convergence and higher overshoot. Hence, in Figure 12.(a), to keep the percent overshoot the same, the convergence times of input current for the P.R. compensator keep increasing as the transition levels are increased

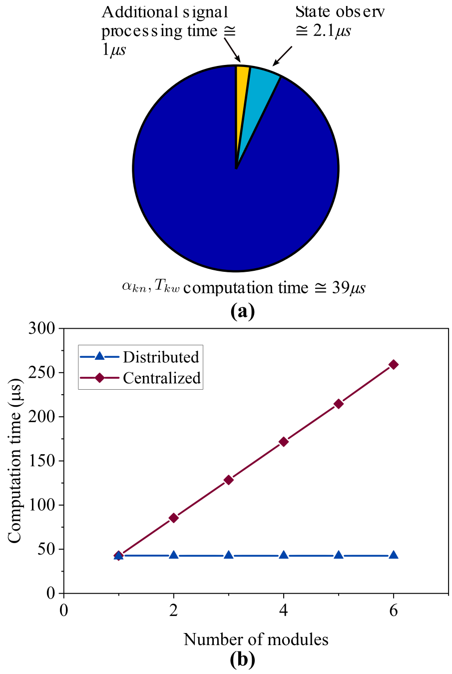

FIGURE 13. (a) Computation times of SBC for a single DMCR module. (b) comparison of the variation of computation times for the centralized and distributed implementation with variation in the number of DMCR modules.

further. On the contrary, SBC maintains fast convergence times even on increased load transition levels. This is mainly due to the faster transient times provided by SBC and due to the full-scale system model used by such controllers for control synthesis. Figure 12.(b) further validates this fact by comparing the peak overshoot of the primary drain to the source voltage of the DMCR to match the SBC transient response with increased load transition levels. As the load transitions become severe, due to shortcomings of the nature of P.R. compensators, it achieves better transient response at the cost of higher overshoots, unlike SBC, which maintains the same response throughout the load transition levels.

Next, like the parallel-connected H-ANPC inverters, the applicability of the standalone DMCR for a network application involving multiple parallel-connected DMCR modules is outlined. The DMCRs in Figure 11 communicate amongst themselves through the same communication interface as that of the parallel H-ANPC inverters. However, contrary to the slower processor used in the SBC execution in the parallel H-ANPC inverters, state-of-the-art dual-core TMS320F28379D has been used to compute the SBC control scheme, that aids the implementation of the SBC in up to 6 PES modules in this illustration case.

Figure 13.(a) shows the computation time taken by SBC to compute the control actions for a single-phase DMCR. For the fundamental switching sequence of the DMCR, the SBC computation time is distributed amongst calculation of the time allocation of the switching states $\{\alpha_{j_{i'}}\}_{i'=1\cdots h_j}$ time horizon T_{w_j} implementation of the state observer for the higher order DMCR and some additional time due to signal processing.

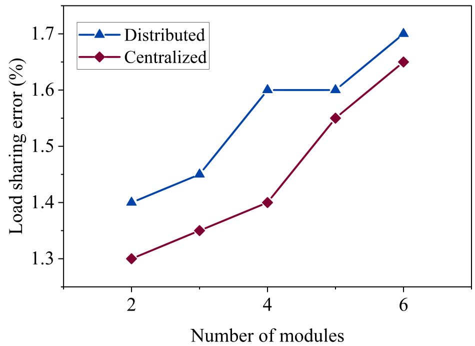

FIGURE 14. Comparison of the load sharing error in centralized and distributed implementation with variation in the number of DMCR modules.

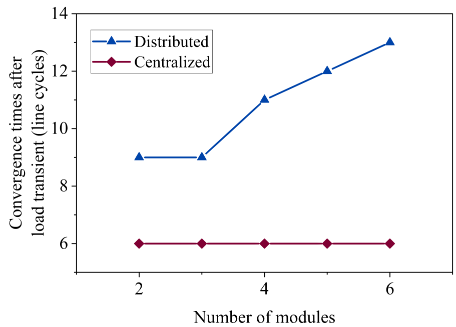

FIGURE 15. Line cycles taken by the input current of the single-phase DMCR input current for centralized and distributed systems to reach a new steady state for an increase in output load demand from 25 A to 50 A.

The networking indeed does additional computation depending on the architecture. Figure 13.(b) shows the increased computation times of the DSP for solving the SBC problem for the parallel DMCRs. As shown, the computation required for the centralized implementation, as shown in Figure 13.(b), increases significantly with an increasing number of modules. Conversely, the computation time required to exchange information and overall cost function analysis for the distributed approach is inferior compared to a centralized approach. However, it comes at the cost of increased communication overhead. To mitigate the latter need, a differential coding technique is adopted to reduce the bit transmission rate [38]. For the above results, notice that the centralized and distributed SBC schemes are implemented on the same processor.

Figure 14 compares the load-sharing error for the centralized and distributed implementations of DMCR control. SBC, in both cases, achieves similar load-sharing performance. The slight increment in load-sharing error in the distributed case is attributed to the different sensor acquisition and calibration in each of the local processors in the distributed system. However, in both cases, SBC achieves tight load regulation and achieves equal sharing.

Figure 15 shows that for the parallel connected DMCR and for the communication protocol under consideration, as the number of parallel modules is increased, the convergence time of the input DMCR current increases as compared to the centralized architecture for a high load transition level

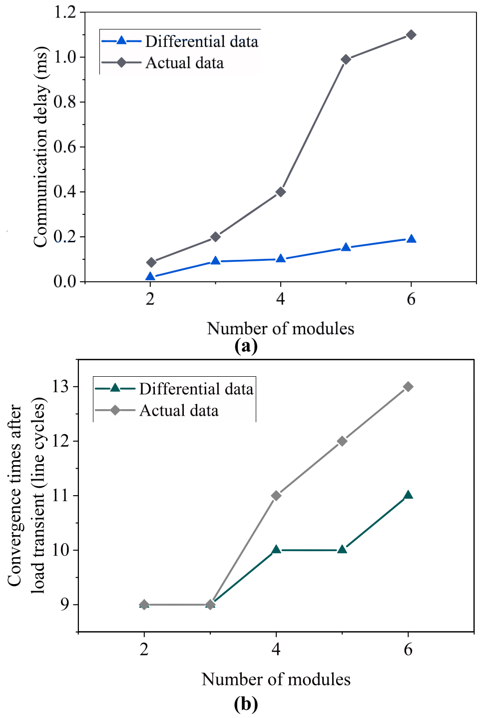

FIGURE 16. **(a) Comparison on the delay between actual and differential data transmission scheme for single phase DMCR with an increasing number of modules. (b) Comparison on the line cycles taken by the input current of the single-phase DMCR input current for the distributed architecture with actual and differential data transmission to reach a new steady state for an increase in output load demand from 25 A to 50 A. The SBC convergence considers 2% nominal overshoot for the distributed architecture.**

from 25 A to 50 A in the DMCR. This is primarily due to communication delay gradually violating stability bounds for such increased transition levels for the higher-order non-minimum phase PES. For the result in Figure 15, we consider the following: the computational power of the centralized system is equivalent to the sum of each of the distributed systems; it is also ensured that there is only 2% nominal overshoot for both the centralized and distributed architectures for Figure 15.

The convergence times can be positively affected by using a differential data transmission scheme for the same communication speed compared to an actual data transmission scheme. Instead of entire data transmission using a limited amount of communication bits, in differential data transfer, the differential information of the change of converter states between two successive communication exchanges is transmitted over the link. This results in increased resolution of the communication variables, thereby positively impacting control performance and convergence times. Figure 16.(a) shows the net communication delay between actual and differential data transfer for the DMCR

with an increasing number of modules connected in parallel. Figure 16.(b) further shows a comparative study of the increased convergence times of the SBC scheme for paralleled DMCRs with an increasing number of modules for differential and actual data transfer. The better performance with differential data transfer is primarily attributed to the higher resolution of exchanged communication variables and reduced communication delay.

V. CONCLUSION

An SBC scheme for networked PES is outlined. While for the standalone PES, the SBC yields robust stability and satisfactory performance [27], for the PES network, the SBC ensures that the performance is within the specified bounds. Guided by solving an optimization problem, SBC essentially controls the evolution of the switching sequences of a PES. These reachable switching sequences can be determined from a set of feasible switching sequences using a multiple-Lyapunov-function-based methodology. As such, this work outlined the mechanism to extend the core SBC for a standalone PES to a PES network using two separate case illustrations.

The efficacy of the proposed SBC framework is validated first for a single-phase standalone and network of parallel H-ANPC inverters and for a single-phase network of CS-PES parallel DMCRs. Irrespective of the topological choice, SBC was able to provide stable PES dynamics and satisfactory PES performance in either mode of operation (standalone/parallel). Compared to the centralized control scheme, the distributed control scheme has a reduced computational complexity but may require greater information exchange. While the centralized implementation scheme indicates to be a viable alternative for a lower number of modules, a distributed/clustered implementation may be desirable for a higher number of PES modules from a computation burden perspective. Nevertheless, in choosing the network architecture, one must consider the dynamic performance of the topological structure, the communication network's bandwidth, the number of modules, and the processing capacity of the control devices. The two different case illustrations also aimed to illustrate that the method is independent of the device choice or semiconductor materials; any wide band gap (WBG) or non-WBG can be used. However, the use of WBG makes the operation more involved due to increased sensor high-frequency noise and differential data transmission amidst that.

The main challenge in applying SBC for networked PES is the scalability of the approach. To scale the control strategy, this paper designed a local SBC just like it would be done for a single standalone PES, but augmented it with low communication overhead (control) information exchanges based on a coding approach. Evidently, the computational burden of combining predictions of the PES modules' future states in the optimization routine's solution (4) also distinguishes the proposed networked SBC control from existing, more uncomplicated control strategies. In this work, the set of feasible switching sequences was computed offline to reduce the computational burden, while the optimization sequence was computed in a single DSP. However, previous work suggests that a combination of digital controller platforms consisting of a DSP and an FPGA can assist in reducing the computational overhead for more convoluted systems [39].

ACKNOWLEDGMENT

The financial support provided by the U.S. Department of Energy's Office of Energy Efficiency and Renewable Energy and by the U.S. National Science Foundation, neither the United States Government nor any agency thereof, nor any of their employees, makes any warranty, express or implied, or assumes any legal liability or responsibility for the accuracy, completeness, or usefulness of any information, apparatus, product, or process disclosed, or represents that its use would not infringe privately owned right.

REFERENCES

[1] S. K. Mazumder and K. Acharya, "Multiple Lyapunov function based reaching condition for orbital existence of switching power converters," *IEEE Trans. Power Electron.*, vol. 23, no. 3, pp. 1449–1471, May 2008.
[2] B. Ferreira, "Understanding the challenges of converter networks and systems: Better opportunities in the future," *IEEE Power Electron. Mag.*, vol. 3, no. 2, pp. 46–49, Jun. 2016, doi: 10.1109/MPEL.2016.2551799.
[3] A. Mohd, E. Ortjohann, D. Morton, and O. Omari, "Review of control techniques for inverters parallel operation," *Electric Power Syst. Res.*, vol. 80, no. 12, pp. 1477–1487, Dec. 2010.
[4] U. De Pra, D. Baert, and H. Kuyken, "Analysis of the degree of reliability of a redundant modular inverter structure," in *Proc. 20th Int. Telecommun. Energy Conf.*, San Francisco, CA, USA, Oct. 1998, pp. 543–548, doi: 10.1109/INTLEC.1998.793592.
[5] T. Kawabata and S. Higashino, "Parallel operation of voltage source inverters," *IEEE Trans. Ind. Appl.*, vol. 24, no. 2, pp. 281–287, Apr. 1988, doi: 10.1109/28.2868.
[6] N. Hur and K. Nam, "A robust load-sharing control scheme for parallel-connected multisystems," *IEEE Trans. Ind. Electron.*, vol. 47, no. 4, pp. 871–879, Aug. 2000, doi: 10.1109/41.857967.
[7] X. Sun, L.-K. Wong, Y.-S. Lee, and D. Xu, "Design and analysis of an optimal controller for parallel multi-inverter systems," *IEEE Trans. Circuits Syst. II, Exp. Briefs*, vol. 53, no. 1, pp. 56–61, Jan. 2006, doi: 10.1109/TCSII.2005.854136.
[8] M. C. Chandorkar, D. M. Divan, and R. Adapa, "Control of parallel connected inverters in standalone AC supply systems," *IEEE Trans. Ind. Appl.*, vol. 29, no. 1, pp. 136–143, Jan./Feb. 1993, doi: 10.1109/28.195899.
[9] C. K. Tse, M. Huang, X. Zhang, D. Liu, and X. L. Li, "Circuits and systems issues in power electronics penetrated power grid," *IEEE Open J. Circuits Syst.*, vol. 1, pp. 140–156, 2020.
[10] S. K. Mazumder and K. Acharya, "Sequence-based control for large-scale power electronics networks," in *Proc. IEEE Power Energy Soc. Gen. Meeting*, Jul. 2009, pp. 1–9, doi: 10.1109/PES.2009.5275896.
[11] X. Wang and F. Blaabjerg, "Harmonic stability in power electronic-based power systems: Concept, modeling, and analysis," *IEEE Trans. Smart Grid*, vol. 10, no. 3, pp. 2858–2870, May 2019, doi: 10.1109/TSG.2018.2812712.
[12] A. Tajfar and S. K. Mazumder, "Sequence-based control of an isolated DC/AC matrix inverter," *IEEE Trans. Power Electron.*, vol. 31, no. 2, pp. 1757–1773, Feb. 2016.
[13] D. Chatterjee and S. K. Mazumder, "Switching-sequence control of a higher order power-electronic system driving a pulsating load," *IEEE Trans. Power Electron.*, vol. 35, no. 1, pp. 1096–1110, Jan. 2020.
[14] J. Chen, J. Wu, K. Liu, R. Wang, W. Li, and X. He, "Improved switching ripple modulation strategy for simultaneous power conversion and data communication in DC–DC converters," *IEEE Trans. Power Electron.*, vol. 37, no. 8, pp. 9275–9284, Aug. 2022, doi: 10.1109/TPEL.2022.3161059.
[15] H. Li, H. Yang, F. Sun, and Y. Xia, "Sliding-mode predictive control of networked control systems under a multiple-packet transmission policy," *IEEE Trans. Ind. Electron.*, vol. 61, no. 11, pp. 6234–6243, Nov. 2014.
[16] H. Komurcugil, "Rotating-sliding-line-based sliding-mode control for single-phase UPS inverters," *IEEE Trans. Ind. Electron.*, vol. 59, no. 10, pp. 3719–3726, Oct. 2012.
[17] J. Rodriguez and P. Cortes, *Predictive Control of Power Converters and Electrical Drives*. Hoboken, NJ, USA: Wiley, 2012.
[18] T. Geyer, *Model Predictive Control of High Power Converters and Industrial Drives*. Hoboken, NJ, USA: Wiley, 2016.
[19] J. B. Rawlings, "Tutorial overview of model predictive control," *IEEE Control Syst.*, vol. 20, no. 3, pp. 38–52, Jun. 2000.
[20] A. Bemporad and M. Morari, "Robust model predictive control: A survey," in *Robustness in Identification and Control* (Lecture Notes in Control and Information Sciences), A. Garulli, A. Tesi, and A. Vicino, Eds. Berlin, Germany: Springer, 1999, pp. 207–226.
[21] R. R. Negenborn, "Multi-agent model predictive control with applications to power networks," Doctoral dissertation, Dept. Elect. Eng., Delft Univ., Delft, The Netherlands, 2007.
[22] S. K. Mazumder, *Wireless Network-Based Control*. Berlin, Germany: Springer, 2010.
[23] D. D. Siljak, *Decentralized Control of Complex Systems*. New York, NY, USA: Academic Press, 1991.
[24] M. Tahir and S. K. Mazumder, "Delay constrained optimal resource utilization of wireless networks for distributed control systems," *IEEE Commun. Lett.*, vol. 12, no. 4, pp. 289–291, Apr. 2008.
[25] M. Tahir and S. K. Mazumder, "Self-triggered communication enabled control of distributed generation in microgrids," *IEEE Trans. Ind. Informat.*, vol. 11, no. 2, pp. 441–449, Apr. 2015.
[26] K. Gu, V. L. Kharitonov, and J. Chen, *Stability of Time Delay Systems*. Boston, MA, USA: Birkhauser, 2003.
[27] S. K. Mazumder and K. Acharya, "Sequence-based control for standalone and networked switching power converters," in *Proc. IEEE Energy Convers. Congr. Expo.*, San Jose, CA, USA, Sep. 2009, pp. 1104–1111, doi: 10.1109/ECCE.2009.5316108.
[28] L. Xu, Q. Guo, Z. Wang, and H. Sun, "Modeling of time-delayed distributed cyber-physical power systems for small-signal stability analysis," *IEEE Trans. Smart Grid*, vol. 12, no. 4, pp. 3425–3437, Jul. 2021, doi: 10.1109/TSG.2021.3052303.
[29] N. Cai and J. Mitra, "A multi-level control architecture for master-slave organized microgrids with power electronic interfaces," *Electric Power Syst. Res.*, vol. 109, pp. 8–19, Apr. 2014.
[30] H. Chen and H.-M. Hansich, "Model aggregation for hierarchical control synthesis of discrete event systems," in *Proc. 39th IEEE Conf. Decis. Control*, Dec. 2000, pp. 418–423.
[31] J. G. Proakis and M. Salehi, *Digital Communications*. New York, NY, USA: McGraw-Hill, 2007.
[32] S. Johannessen, "Time synchronization in a local area network," *IEEE Control Syst.*, vol. 24, no. 2, pp. 61–69, Apr. 2004.
[33] A. Ingalalli and S. Kamalasadan, "Decentralized state estimation-based optimal integral model predictive control of voltage and frequency in the distribution system microgrids," *IEEE Trans. Smart Grid*, vol. 14, no. 3, pp. 1790–1803, May 2023, doi: 10.1109/TSG.2022.3220714.
[34] B.-S. Ko, G.-Y. Lee, K.-Y. Choi, R.-Y. Kim, S. Kim, J. Cho, and S.-I. Kim, "Flexible control structure for enhancement of scalability in DC microgrids," *IEEE Syst. J.*, vol. 14, no. 3, pp. 4591–4601, Sep. 2020, doi: 10.1109/JSYST.2019.2963707.
[35] S. Boyd and L. Vandenberghe, *Convex Optimization*. New York, NY, USA: Cambridge Univ. Press, 2004.
[36] E. K. P. Chong and S. H. Zak, *An Introduction to Optimization*. New York, NY, USA: Wiley, 2001.
[37] R. Teodorescu, F. Blaabjerg, M. Liserre, and P. C. Loh, "Proportional-resonant controllers and filters for grid-connected voltage-source converters," *IEE Proc.-Electr. Power Appl.*, vol. 153, no. 5, pp. 750–762, Sep. 2006.
[38] S. K. Mazumder, K. Acharya, and M. Tahir, "Towards realization of a control-commnunication framework for interactive power networks," in *Proc. IEEE Energy Conf.*, Atlanta, GA, USA, Nov. 2008, pp. 1–8, doi: 10.1109/ENERGY.2008.4781037.
[39] S. K. Mazumder, K. Acharya, and M. Tahir, "Joint optimization of control performance and network resource utilization in homogeneous power networks," *IEEE Trans. Ind. Electron.*, vol. 56, no. 5, pp. 1736–1745, May 2009, doi: 10.1109/TIE.2009.2012458.

MATEO D. ROIG GREIDANUS (Graduate Student Member, IEEE) received the B.E. and M.S. degree in electrical engineering from the Federal University of Santa Catarina (UFSC), Florianópolis, Brazil, in 2018 and 2020, respectively. He is currently pursuing the Ph.D. degree in electrical and computer engineering with the Laboratory for Energy and Switching-Electronic Systems (LESES), University of Illinois Chicago (UIC), Chicago, IL, USA. His research interests include modeling, optimal control, non-linear analysis, stability of power electronic systems, renewable energy integration, and cyber-physical security of power electronic-dominated grids.

SUDIP K. MAZUMDER (Fellow, IEEE) received the Ph.D. degree in electrical and computer engineering from Virginia Tech, in 2001.

He has been the President of NextWatt LLC, since 2008. He has been a Professor with UIC, since 2001. He has more than 30 years of professional experience and has held research and development and design positions in leading industrial organizations and has served as a technical consultant for several industries. Dr. Mazumder was named a fellow of the American Association for the Advancement of Science (AAAS), in 2020, the Institute of Electrical and Electronics Engineers (IEEE), in 2016, and the Asia-Pacific Artificial Intelligence Association (AAIA), in 2022. He has been serving as an Administrative Committee Member for IEEE PELS, since 2015. He has been serving as a Member-at-Large for IEEE PELS, since 2020. In June 2023, he was a recipient of the Honorary Title of UIC Distinguished Professor to be effective in AY'23 pending Board of Trustees approval. He was a recipient of the 2023 IEEE Power and Energy Society's Ramakumar Family Renewable Energy Excellence Award. He received several IEEE awards/honors, including the IEEE Transactions on Power Electronics Prize Paper Awards, in 2002 and 2022, the Highlighted Papers, in 2018, 2022, and 2023, the Featured Article for IEEE Transactions on Biomedical Engineering, in 2023, the IEEE Conference Best Paper Award, in 2013, and the IEEE International Future Energy Challenge Award, in 2005. He was a recipient of the most prestigious awards at UIC, including the Distinguished Researcher Award in Natural Sciences and Engineering, in 2020, the Inventor of the Year Award, in 2014, and the University Scholar Award, in 2013. Earlier, he received the prestigious U.S. Office of Naval Research (ONR) Young Investigator Award, in 2005, and the U.S. National Science Foundation (NSF) CAREER Award, in 2003. He served as the Chair for the IEEE PELS Technical Committee on Sustainable Energy Systems, from 2015 to 2020. He serves as the General Chair for IEEE PEDG Conference, in 2023. He has been serving as an Editor-in-Large for the IEEE Transactions on Power Electronics, since 2019. He served as an IEEE Distinguished Lecturer, from 2016 to 2019. He has also made original contributions to the areas of control of power-electronic systems at the semiconductor device level for numerous and wide-ranging applications in commercial and defense space; high-frequency-link power electronics, including hybrid-modulation-based pulsating-dc-link inverter and differential-mode-converter (ac/ac, dc/ac, ac/dc) topologies for applications encompassing but not limited to renewable and alternative energy, electric vehicles, solid-state transformer, energy storage, and offshore wind; discretized high-frequency and Boolean energy and data transfer; and optically-controlled power semiconductor devices (including optical emitter turn-off thyristor, heterojunction devices, high-gain bipolar devices, and hybrid and monolithic photoconductive semiconductor switches (PCSS)) and power electronics.

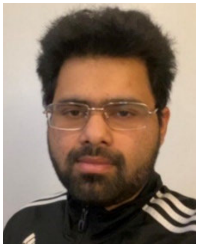

DEBANJAN CHATTERJEE (Member, IEEE) received the B.E. degree in electrical engineering from Jadavpur University, Kolkata, India, in 2015, and the Ph.D. degree in electrical and computer engineering from the University of Illinois Chicago (UIC), Chicago, IL, USA, in 2021. He has been with the ABB US Research Center (USRC), Raleigh, since July 2021, where he is working on power electronic applications for ABB robotics, electrification, and motion. His research interests include encompass design, control, and protection of wideband gap power electronic systems.

MUHAMMAD TAHIR (Member, IEEE) received the Ph.D. degree in electrical and computer engineering from the University of Illinois Chicago, Chicago, IL, USA, in 2008. He was a Visiting Research Scholar with the University of Illinois Chicago, in the summer of 2014. He is currently a Professor with the Department of Electrical Engineering, University of Engineering and Technology at Lahore, Lahore, Pakistan. He has more than 60 international publications to his credit. He has served as a principal investigator for numerous funded research projects related to embedded systems and intelligent surveillance networks. His research interests include distributed resource optimization for wireless networks, real-time wireless multimedia networks and computer architecture. He is a reviewer of numerous IEEE journals and conferences.

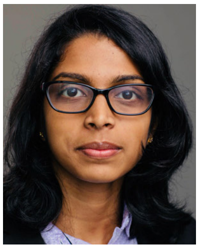

NANDITHA GAJANUR (Graduate Student Member, IEEE) received the B.Tech. degree in electronics engineering from Manipal Institute of Technology, Manipal, India, in 2017, and the M.S. degree in electrical and computer engineering from The Ohio State University, Columbus, OH, USA, in 2019. She is currently pursuing the Ph.D. degree in electrical and computer engineering with the Laboratory for Energy and Switching-Electronic Systems (LESES), University of Illinois Chicago (UIC), Chicago, IL, USA. Her research interests include modeling, analysis, and reliability-oriented control of power electronic systems and cyber-security of power converters for renewable energy resources.